Mechanics of Advanced Composite Structures 9 (2022) 49 – 57

Semnan University

Mechanics of Advanced Composite Structures

journal homepage: http://MACS.journals.semnan.ac.ir

Transient Solution of Heat and Moisture Transfer in a Functionally Graded Hollow Cylinder with Finite Length

M. Saadatfar*

Department of Mechanical Engineering, Faculty of Engineering, University of Qom, Qom, Iran

KEYWORDS

Transient hygrothermal;
Coupled temperature and moisture;
FGM;
Hollow cylinder;
DQM;

ABSTRACT

In this article, temperature and moisture distributions in a finite-length hollow cylinder made of functionally graded material (FGM) under transient coupled hygrothermal condition was presented. The coupled equations of heat conduction and moisture diffusion were solved employing the Fourier series expansion method along the longitudinal direction, the differential quadrature method (DQM) along the radial direction, and the Newmark method for the time domain. Finally, the history of temperature and moisture potentials was obtained. The effect of coupled and uncoupled hygrothermal loading, grading index, and hygrothermal boundary conditions was illustrated in numerical examples. Results show that the difference between the coupled model and uncoupled model is more obvious in the moisture rather than the temperature. Also, the negative grading index increases the temperature and moisture. While the effect of the positive grading index is vice versa. Moreover, to have a more accurate analysis of the transient hygrothermal process, it is important to employ the coupled model.

1. Introduction

FGMs have been employed in industrial structures owing to their excellent thermomechanical properties. FGM refers to the materials whose properties vary gradually from one side to another side and are mostly used where the high thermal gradient exists. The idea of FGM is proper to various engineering areas such as nuclear energy, aerospace vehicle, chemical plant, and electronics [1-3]. In the last decade, many researchers tried to study the behavior of FGMs in various environmental conditions. Due to usages of industrial structures subjected to various environmental conditions and loads, disclosing the influence of humidity and thermal environment on their behavior is a new topic in the literature.

Using a finite element-finite difference method, transient temperature distribution and thermal stresses in FGMs were presented by Wang et al. [4]. Jabbari et al. [5] studied the three-dimensional thermo-mechanical stresses in FGM short hollow cylinders. Shao et al. [6] investigated thermo-elastic analysis of FGM hollow cylinders under axisymmetric mechanical and transient thermal loads. Ootao and Tanigawa [7] analyzed a transient thermoelastic problem in an FGM hollow cylinder subjected to asymmetrical heating from its surfaces. Transient heat conduction in two-dimensional FGM short hollow cylinders was analyzed by Asghari and Akhlaghi [8]. Peng and Li [9] investigated the transient response of temperature distribution and thermal stresses in an FGM hollow cylinder. Using a multi-layered approach, the solution of temperature in FGM hollow cylinders under transient thermal boundary conditions was presented by presented Rahmati Nezhad et al. [10]. Using finite difference and Newmark methods, the two-dimensional thermo-mechanical dynamic behavior of a long hollow FGM cylinder under asymmetrical thermo-mechanical loads was studied by Xie et al. [11]. Nejad and Kashkoli [12] presented time-dependent thermo-mechanical creep analysis for a rotating hollow cylinder made of FGM. Hosseini and Dini [13] developed an analytical solution for the problem of stress analysis of rotating thick-walled FGM cylinders under the magnetic field and thermal loads at the plane strain state. Using

* Corresponding author. Tel.: +98-25-32103577
E-mail address: m.saadatfar@gmail.com; m.Saadatfar@qom.ac.ir

DOI: 10.22075/macs.2022.24225.1355
Received 2021-08-12 ; Received in revised form 2021-10-06 ; Accepted 2022-01-01.

DQM, Hosseini et al. [14] investigated strain gradient effects on the thermoelastic analysis of a micro-rotating FGM cylinder. The transient thermo-mechanical behavior of a short hollow cylinder made of two-dimensional FGM was investigated by Najibi and Talebitooti [15]. Manthena and Kedar [16] considered the thermal stresses of a thick-walled hollow FGM cylinder with temperature dependent material properties. Using an analytical method, the problem of time-dependent behavior of a functionally graded magneto-electro-elastic rotating hollow cylinder in a thermal environment was analyzed by Saadatfar [17]. Yarimpabuc obtained a closed-form solution for transient thermal stress response of an FGM hollow cylinder subjected to temperature gradient under a periodic rotation [18]. A thermo-elastic analysis for rotating FGM cylindrical shells with variable thickness under thermo-mechanical loading was presented by Jabbari and Zamani Nejad [19]. Based on the strain gradient theory, Dini et al. [20] presented a size-dependent analysis of the FGPM micro-rotating cylinder at the plane strain condition. Benslimane et al. [21] developed an analytical solution to evaluate stresses and deformations in a thick-walled cylindrical shell made of FGM.

Analysis of cylinders and cylindrical shells made of multilayered composites, FGMs, and smart materials in the hygrothermal environmental condition is of interest for many researchers. Saadatfar and Aghaie-Khafri [22] evaluated the hygrothermal stresses and deformations in a functionally graded magneto-electro-elastic (FGMEE) hollow sphere by means of an analytical method. Saadatfar and Aghaie Khafri [23] analyzed a smart cylindrical shell with FGM core and FGPM layers subjected to hygrothermal loading. They explained that the grading index has a significant effect of the actuation and sensing authority of FGPM layers subjected to multifield loading. Then, Saadatfar and Aghaie-Khafri analyzed the hygro-thermo-electro-elastic [24] response of a cylindrical shell made of FGM integrated with FGPM layers. Later, hygro-thermo-magneto-electro-elastic analysis of this problem was presented by saadatfar [25, 26]. Dini and Abolbashari [27] analyzed a hollow FGPM cylinder under a non-axisymmetric hygro-thermo-electro-elastic loading. Saadatfar [28] investigated the history of displacement, stresses, electric potential, and magnetic potential of an FGMEE hollow cylinder under an axisymmetric hygro-thermo-magneto-electro-mechanical loading for the plane strain condition. Saadatfar [29] presented an analytical solution for the problem of the time-dependent response of a piezomagnetic rotating hollow cylinder under an axisymmetric multiphysical loading for the plane strain state.

Due to the complexity of coupled hygrothermal equations, the uncoupled hygrothermal equations have been supposed in most of the published articles. However, coupled hygrothermal equations for temperature and moisture should be considered to have an accurate evaluation for transient temperature distribution as well as moisture potential distribution. Using Laplace transformation and the finite difference method, Yang et al. [30] solved the transient coupled hygrothermal problem of a long cylinder. The distributions of the temperature, moisture, deformation, and stress of a rotating FGPM disk subjected to coupled hygrothermal loading were presented by Dai et al. [31]. Dai et al. [32] presented a mechanical model to study the coupled hygrothermal behavior of a variable thickness rotating porous disk made of functionally graded carbon nanotube reinforced composite. The transient coupled hygrothermal and mechanical behavior of a long cylinder under sudden hygrothermal loadings was studied by Peng et al. [33]. Peng et al. [34] analyzed the transient response of a porous long cylinder subjected to coupled hygrothermal condition.

Literature review reveals that there is not any reported work on transient responses of a short-length FGM cylinder subjected to coupled hygrothermal condition. So, for the first time, the coupled equations of heat conduction and moisture diffusion were considered for short-length FGM cylinder. The equations were solved using the Fourier series expansion method, DQM, and Newmark method. The distribution of temperature and moisture was obtained through time and radius. The effects of various parameters were investigated comprehensively in the numerical section.

2. Coupled Heat and Moisture Transfer

Consider a short hollow cylinder with length L and inner and outer radii a and b, respectively. The cylinder is placed in a hygrothermal field and rotates around its axis with constant angular velocity. For the sake of simplifying, the material constants of the FGM are assumed to vary according to power-law function through the radial direction as:

$$Y = Y'\left(\frac{r}{a}\right)^{\beta}, Y = k, \rho, \zeta, c_p, c_m \quad (1)$$

where, Y and Y' are material constants and corresponding values at the inside radius, respectively.

2.1. Basic Equations

The coupled hygrothermal equations can be written as follows [35]:

$$\nabla.(k\nabla T)+\rho c_m(\xi_D h_{LV}+\gamma)\frac{\partial M}{\partial t}=\rho c_p\frac{\partial T}{\partial t} \quad (2)$$

$$\rho c_m\frac{\partial M}{\partial t}=\nabla.(\zeta\nabla M)+\nabla.(\varepsilon\zeta\nabla T) \quad (3)$$

Considering the cylindrical coordinate system, the Eqs. (2)-(3) can be rewritten as:

$$\begin{aligned}&\frac{1}{r}\frac{\partial}{\partial r}\left(rk_r\frac{\partial T}{\partial r}\right)+\frac{1}{r^2}\frac{\partial}{\partial\theta}\left(k_\theta\frac{\partial T}{\partial\theta}\right)+\frac{\partial}{\partial z}\left(k_z\frac{\partial T}{\partial z}\right)\\&=\rho c_p\frac{\partial T}{\partial t}-[\rho c_m(\xi_D\,h_{LV}+\gamma)]\frac{\partial M}{\partial t}\end{aligned} \quad (4)$$

$$\begin{aligned}&\frac{1}{r}\frac{\partial}{\partial r}\left(r\zeta_r\frac{\partial M}{\partial r}\right)+\frac{1}{r^2}\frac{\partial}{\partial\theta}\left(\zeta_\theta\frac{\partial M}{\partial\theta}\right)\\&+\frac{\partial}{\partial z}\left(\zeta_z\frac{\partial M}{\partial z}\right)+\frac{1}{r}\frac{\partial}{\partial r}\left(r\varepsilon\zeta_r\frac{\partial T}{\partial r}\right)\\&+\frac{1}{r^2}\frac{\partial}{\partial\theta}\left(\varepsilon\zeta_\theta\frac{\partial T}{\partial\theta}\right)+\frac{\partial}{\partial z}\left(\varepsilon\zeta_z\frac{\partial T}{\partial z}\right)=\rho c_m\frac{\partial M}{\partial t}\end{aligned} \quad (5)$$

Due to the axisymmetric condition, the terms include derivative respect to θ is vanished. Using Eq.(1), one has:

$$\begin{aligned}&\left(k_r'\left(\frac{\partial^2}{\partial r^2}+\frac{\beta+1}{r}\frac{\partial}{\partial r}\right)+k_z'\frac{\partial^2}{\partial z^2}\right)T\\&=\left(\frac{r}{a}\right)^\beta\rho'c_p'\frac{\partial T}{\partial t}-\left(\frac{r}{a}\right)^\beta\rho'c_m'(\xi_D\,h_{LV}+\gamma)\frac{\partial M}{\partial t}\end{aligned} \quad (6)$$

$$\begin{aligned}&\left(\zeta_r'\left(\frac{\partial^2}{\partial r^2}+\frac{\beta+1}{r}\frac{\partial}{\partial r}\right)+\zeta_z'\frac{\partial^2}{\partial z^2}\right)M\\&+\left(\varepsilon\zeta_r'\left(\frac{\partial^2}{\partial r^2}+\frac{\beta+1}{r}\frac{\partial}{\partial r}\right)+\varepsilon\zeta_z'\frac{\partial^2}{\partial z^2}\right)T\\&=\left(\frac{r}{a}\right)^\beta\rho'c_m'\frac{\partial M}{\partial t}\end{aligned} \quad (7)$$

The initial conditions of the hygrothermal field are considered as:

$$T(r,z,0)=0,\qquad M(r,z,0)=0 \quad (8)$$

The boundary conditions of the hygrothermal field can be considered as:

$$\begin{aligned}&T(a,z,t)=T_a,\qquad T(b,z,t)=T_b\\&M(a,z,t)=M_a,\qquad M(b,z,t)=M_b\\&T(r,0,t)=0,\qquad T(r,L,t)=0\\&M(r,0,t)=0,\qquad M(r,L,t)=0\end{aligned} \quad (9)$$

2.2. Solution Method

The solutions of the coupled hygrothermal problem satisfying the temperature and moisture concentration boundary conditions at the end faces can be considered as:

$$\begin{aligned}T(r,z,t)&=\sum_{n=1}^{\infty}\bar{T}_n(r,t)\,sin(p_nz)\\M(r,z,t)&=\sum_{n=1}^{\infty}\bar{M}_n(r,t)\,sin(p_nz)\end{aligned} \quad (10)$$

where $p_n=n\pi/L$. Using Eq.(10), the Eqs. (6)-(7) can be rewritten as:

$$\begin{aligned}&\left(k_r'\left(\frac{\partial^2}{\partial r^2}+\frac{\beta+1}{r}\frac{\partial}{\partial r}\right)-k_z'p_n^2\right)\bar{T}=\\&\left(\frac{r}{a}\right)^\beta\rho'c_p'\frac{\partial\bar{T}}{\partial t}-\left(\frac{r}{a}\right)^\beta\rho'c_m'(\xi_D\,h_{LV}+\gamma)\frac{\partial\bar{M}}{\partial t}\end{aligned} \quad (11)$$

$$\begin{aligned}&\left(\zeta_r'\left(\frac{\partial^2}{\partial r^2}+\frac{\beta+1}{r}\frac{\partial}{\partial r}\right)-\zeta_z'p_n^2\right)\bar{M}\\&+\left(\varepsilon\zeta_r'\left(\frac{\partial^2}{\partial r^2}+\frac{\beta+1}{r}\frac{\partial}{\partial r}\right)-\varepsilon\zeta_z'p_n^2\right)\bar{T}\\&=\left(\frac{r}{a}\right)^\beta\rho'c_m'\frac{\partial\bar{M}}{\partial t}\end{aligned} \quad (12)$$

Using the following formulation based on DQM, the n_{th}-order derivative of the function f(x) at any sample point can be approximated as:

$$\begin{aligned}&\frac{d^nf(x_j)}{dx^n}=\sum_{j=1}^{N}A_{ij}^{(n)}f(x_j),\\&i,j=1\dots N,\qquad n=1\dots N-1\end{aligned} \quad (13)$$

where, $A_{ij}^{(n)}$ are the weighting coefficients used for the n_{th}-order derivatives, and N is the number of grid points along the x direction. Employing the Lagrange interpolation polynomials as approximating functions, the following algebraic relations can be used to evaluate the first and the second order weighting coefficients:

$$\begin{aligned}&A_{ij}^{(1)}=\frac{\Pi(x_i)}{(x_i-x_j).\Pi(x_j)}\qquad i,j=1,\dots,N\ \&j\neq i\\&A_{ij}^{(2)}=2\left[A_{ii}^{(1)}.A_{ij}^{(1)}-\frac{A_{ij}^{(1)}}{x_i-x_j}\right]\quad 2\le n\le N-1\\&A_{ii}^{(1)}=-\sum_{j=1j\neq i}^{N}A_{ij}^{(1)}\qquad k=1,\dots,N-1\\&\Pi(x_i)=\prod_{j=1j\neq i}^{N}(x_i-x_j)\end{aligned} \quad (14)$$

For numerical computation, the Chebyshev–Gauss–Lobatto points with the following coordinates are used:

$$x_i=\frac{L}{2}\left(1-cos\left[\frac{(i-1)\pi}{(N-1)}\right]\right)i=1,2,3,\dots,N \quad (15)$$

Using DQM, the equations of coupled thermal and moisture concentration fields can be written as:

$$k_r'\left(\sum_{j=1}^{N} A_{ij}^{(2)} + \frac{\beta+1}{r_i}\sum_{j=1}^{N} A_{ij}^{(1)}\right)\bar{T}_j - k_z' p_n^2 \bar{T}_i = \left(\frac{r_i}{a}\right)^{\beta} \rho' c_p' \frac{\partial \bar{T}_i}{\partial t} - \left(\frac{r_i}{a}\right)^{\beta} \rho' c_m' (\xi_D\, h_{LV} + \gamma)\frac{\partial \bar{M}_i}{\partial t} \quad (16)$$

$$\zeta_r'\left(\sum_{j=1}^{N} A_{ij}^{(2)} + \frac{\beta+1}{r_i}\sum_{j=1}^{N} A_{ij}^{(1)}\right)\bar{M}_j - \zeta_z' p_n^2 \bar{M}_i + \varepsilon\zeta_r'\left(\sum_{j=1}^{N} A_{ij}^{(2)} + \frac{\beta+1}{r_i}\sum_{j=1}^{N} A_{ij}^{(1)}\right)\bar{T}_j - \varepsilon\zeta_z' p_n^2 \bar{T}_i = \left(\frac{r_i}{a}\right)^{\beta} \rho' c_m' \frac{\partial \bar{M}_i}{\partial t} \quad (17)$$

Now the Newmark method is selected for discretizing the time domain. Divide the time domain by time step Δt. According to the Newmark method, the function $U(r,t)$ and its derivatives with respect to time can be approximated by:

$$\begin{aligned} &\ddot{U}(r_i, t_{i+1}) = a_0\big(U(r_i, t_{i+1}) - U(r_i, t_i)\big) - a_1\dot{U}(r_i, t_i) - a_2\ddot{U}(r_i, t_i)\\ &\dot{U}(r_i, t_{i+1}) = \dot{U}(r_i, t_i) + a_3\ddot{U}(r_i, t_i) + a_4\ddot{U}(r_i, t_{i+1})\\ &a_0 = \frac{1}{\alpha_0 \Delta t^2}, a_1 = \frac{1}{\alpha_0 \Delta t}, a_2 = \frac{1}{2\alpha_0} - 1,\\ &a_3 = \Delta t(1-\delta_0), \qquad a_4 = \delta_0 \Delta t \end{aligned} \quad (18)$$

where α_0=1/4 and δ_0=1/2 are used. Now, Eqs.(16)-(17) can be rewritten in the form as:

$$\begin{aligned} &k_r'\Big(\sum_{j=1}^{N} A_{ij}^{(2)} + \frac{\beta+1}{r_i}\sum_{j=1}^{N} A_{ij}^{(1)}\Big)\bar{T}_j(t_{k+1}) - (k_z' p_n^2 + a_4 a_0 (\frac{r_i}{a})^{\beta}\rho' c_p')\bar{T}_i(t_{k+1})\\ &+ a_4 a_0 (\frac{r_i}{a})^{\beta}\rho' c_m'(\xi_D\, h_{LV} + \gamma)\bar{M}_i(t_{k+1})\\ &= (\frac{r_i}{a})^{\beta}\rho' c_p'(\dot{\bar{T}}_i(t_k) + a_3\ddot{\bar{T}}_i(t_k) - a_4 a_0 \bar{T}_i(t_k)\\ &- a_4 a_1 \dot{\bar{T}}_i(t_k) - a_4 a_2 \ddot{\bar{T}}_i(t_k))\\ &- (\frac{r_i}{a})^{\beta}\rho' c_m'(\xi_D\, h_{LV} + \gamma)(\dot{\bar{M}}_i(t_k) + a_3\ddot{\bar{M}}_i(t_k)\\ &- a_4 a_0 \bar{M}_i(t_k) - a_4 a_1 \dot{\bar{M}}_i(t_k) - a_4 a_2 \ddot{\bar{M}}_i(t_k)) \end{aligned} \quad (19)$$

$$\begin{aligned} &\zeta_r'\left(\sum_{j=1}^{N} A_{ij}^{(2)} + \frac{\beta+1}{r_i}\sum_{j=1}^{N} A_{ij}^{(1)}\right)\bar{M}_j(t_{k+1}) - \left(\zeta_z' p_n^2 + a_4 a_0 \left(\frac{r_i}{a}\right)^{\beta}\rho' c_m'\right)\bar{M}_i(t_{k+1})\\ &+ \varepsilon\zeta_r'\left(\sum_{j=1}^{N} A_{ij}^{(2)} + \frac{\beta+1}{r_i}\sum_{j=1}^{N} A_{ij}^{(1)}\right)\bar{T}_j(t_{k+1}) - \varepsilon\zeta_z' p_n^2 \bar{T}_i(t_{k+1}) = (\frac{r_i}{a})^{\beta}\rho' c_m'(\dot{\bar{M}}_i(t_k)\\ &+ a_3\ddot{\bar{M}}_i(t_k) - a_4 a_0 \bar{M}_i(t_k)\\ &- a_4 a_1 \dot{\bar{M}}_i(t_k) - a_4 a_2 \ddot{\bar{M}}_i(t_k)) \end{aligned} \quad (20)$$

Now, a system of linear algebraic equations is obtained in each time step which can be solved using an iterative method. Domain and boundary degrees of freedom should be separated. They are indicated as (d) and (b) in vector forms, respectively. Accordingly, the matrix form of governing equations and boundary conditions can be expressed as:

$$\begin{bmatrix}[Q_{bb}] & [Q_{bd}]\\ [Q_{db}] & [Q_{dd}]\end{bmatrix}\begin{Bmatrix}\{Z_b\}\\ \{Z_d\}\end{Bmatrix} = \begin{Bmatrix}\{F_b\}\\ \{F_d\}\end{Bmatrix} \quad (21)$$

where:

$$\{Z_b\} = \{\{T_b\}, \{M_b\}\}^T \qquad \{Z_d\} = \{\{T_d\}, \{M_d\}\}^T \quad (22)$$

By eliminating the column vector Z_b; the matrix Eq.(19) is reduced to the following system of algebraic equations:

$$[Q]\{Z_d\} = \{F\} \qquad [Q] = [Q_{dd}] - [Q_{db}][Q_{bb}]^{-1}[Q_{bd}] \qquad \{F\} = \{F_d\} - [Q_{db}][Q_{bb}]^{-1}\{F_b\} \quad (23)$$

Employing direct or iterative methods, Eq.(23) can be solved as a system of algebraic equations. The direct methods may not be efficient for the large system of algebraic equations. In this case, employing iterative methods such as the Gauss-Seidel method is suggested.

3. Numerical Results and Discussion

To disclose the effects of different parameters on the transient behavior of the FGM hollow cylinder, some numerical examples are presented in this section. Material constants to be used for the FGM cylinder are in Table 1 [31, 33, 36]. The length, inside radius, and outside radius of the hollow cylinder are considered as L =1.5m a=0.2m and b=0.25m. To have accurate results, 27 nodes are considered through the thickness for DQM. The following non-dimensional quantities are used in the results:

$$R = \frac{r-a}{b-a}, \qquad T^* = \frac{T}{T_a}, \qquad M^* = \frac{M}{M_a} \quad (24)$$

To the best of author's knowledge, there is no available paper in the literature for transient coupled hygrothermal analysis of FGM cylinders. So, the results were compared with reported results for a FGM cylinder subjected to transient thermal loading. The temperature distribution through the time was compared with Ref. [10]. In this case we have: r_a=0.5m, r_b=1m, L=1.5m, T_a=100(1-e^{-2t}), T_b=0. The used material constants can be found in the cited reference. The results are shown in Fig.1 As illustrated, the graphs show good agreement between the results.

Table 1. Material constants

Parameter	Value	Parameter	Value
C_p(J/kg K)	700	ξ_d	0.3
k(W/mk)	18.1	γ	0
α (1/K)	10.3×10^{-6}	ρ (kg/m^3)	5300
h_{LV} (kJ/kg)	2500	ζ_i (kg/ms°M)	1.73×10^{-8}
ε (°M/K)	2	C_m(J/kg°M)	0.01

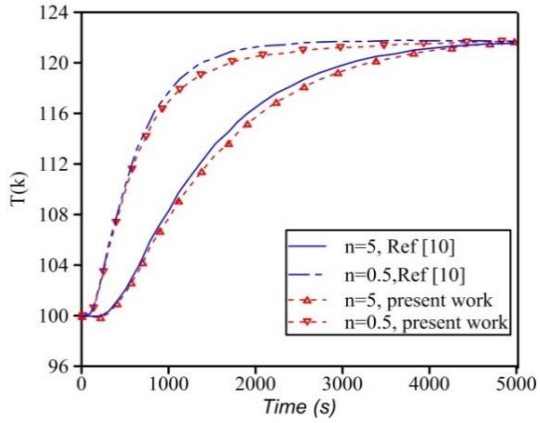

Fig. 1. Distribution of temperature along time

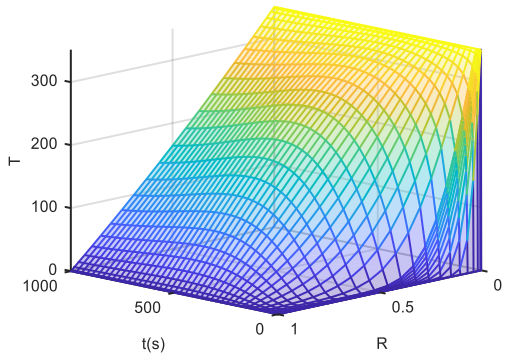

(a)

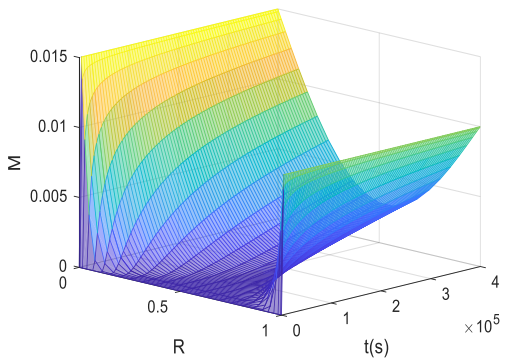

(b)

Fig. 2. Distribution of (a) Tmeperature and (b) Moisture for β=0.5

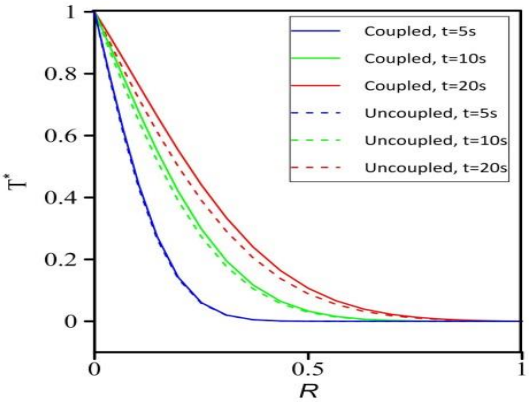

(a)

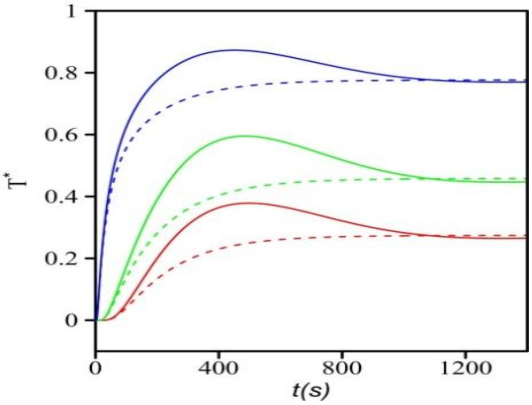

(b)

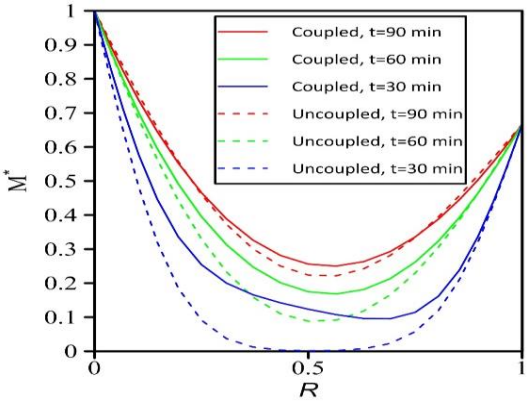

(c)

Fig. 3. Distribution of (a) temperature along radius, (b) temperature along time and (c) moisture along radius, β=0.5

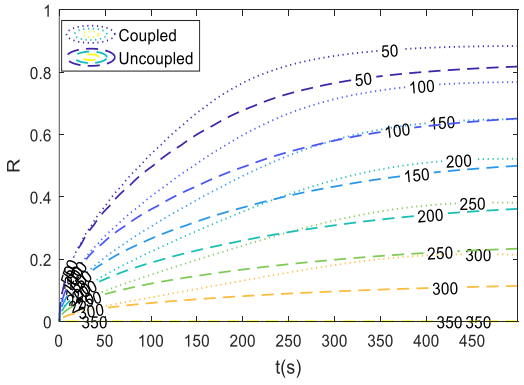

Fig. 4. Distribution of temperature, β=0.5

The distribution of temperature and moisture concentration is studied now. In this case we have: T_a=350K, T_b=0K, M_a=0.015wt%, M_b=0.01wt%. To have a better understanding of changes through time, Fig. 2 shows the heat transfer and moisture diffusion along the radius and time (coupled model). It is observed that the boundary conditions, as well as initial conditions, are satisfied completely. For the next case, the difference between coupled model and the uncoupled model should be investigated. Fig. 3(a) shows the distribution of temperature along the radius. It shows that there is little difference between coupled hygrothermal with uncoupled model in temperature distribution. Fig. 3(b) shows the temperature distribution through time. Fig. 3(b) demonstrates that the FGM cylinder reaches the temperature balance earlier using the uncoupled model, and the temperature before balance increases with time. Using the coupled model, the time to reach the balance is longer and the temperature before the balance first increases and then decreases. Before reaching the balance, the temperature under the uncoupled model is lower than that by the coupled model. Fig. 3(c) depicts the distribution of moisture along the radius. It can be seen that the difference between a coupled model with an uncoupled model is more obvious in moisture rather than temperature. The difference becomes smaller by increasing the time.

For better understanding, Fig. 4 helps better understanding about difference between coupled and uncoupled model and the distribution of temperature along time and radius. Each line indicates the level of temperature that is denoted by a number above the line. Fig. 4 shows that the temperature transfers from inner radius to outer radius by serving the time. Each fixed point on the radius reaches the temperature levels earlier using the coupled model rather than the uncoupled model. Also, at a fixed time, the temperature transfers to a larger part of thickness using the coupled model rather than the uncoupled model.

Regarding the difference between the results under coupled and uncoupled model, for analyzing the transient conduction process it is vital to employ the coupled model. However, after the balance state, using the coupled model or uncoupled model has little effect.

The grading index is the next parameter that its effect was investigated. The effect of the grading index is demonstrated in Fig. 5 and Fig. 6. The boundary conditions are as previous. According to Fig. 5, the negative grading index increases the temperature and moisture at the same point, while the effect of the positive grading index is vice versa. Also, the negative grading index increases the balance temperature and the positive grading index reduces the balance temperature.

Fig. 6 shows the contour of heat transfer and moisture diffusion along time and radius for different grading indexes. It is observed that, similar to Fig. 5, using the negative grading index results in higher temperature transfer and moisture diffusion, and using the negative one has a reverse effect. According to Fig. 6(a), Each fixed point on the radius reaches the temperature levels earlier using a negative grading index. However, the effect of the positive grading index is vice versa. Also, at a fixed time, the temperature transfers to a larger part of thickness using the negative grading index. Whereas, a positive grading index has a reverse effect. According to Fig. 6(b), the effect of the grading index on the moisture transfer is similar to the temperature transfer.

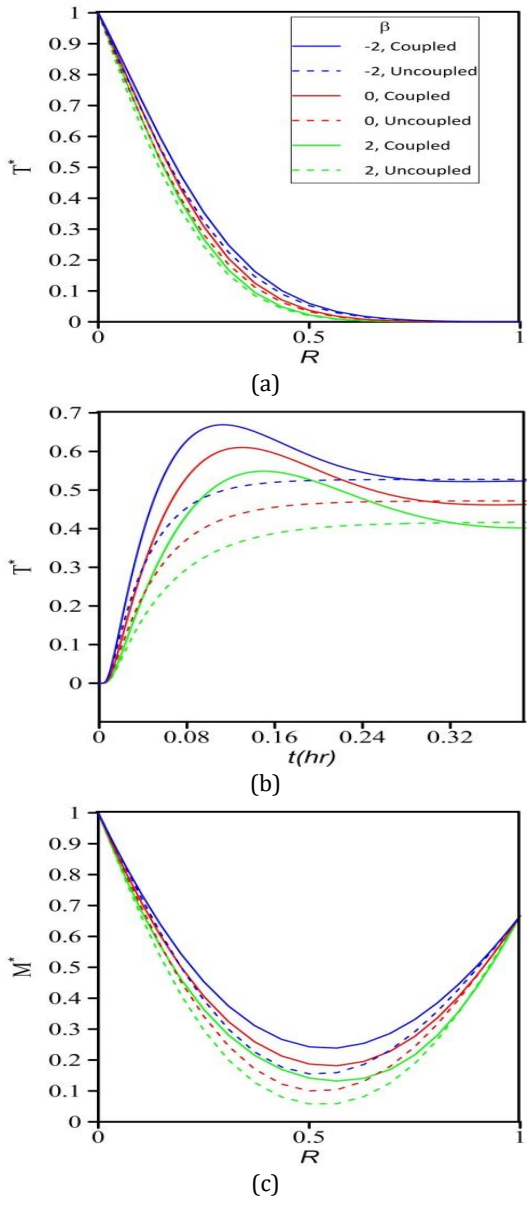

Fig. 5. Effect of inhomogeneity index on the distribution of (a) temperature along radius (t=15s), (b) temperature along the time and (c) moisture along radius (t=100min).

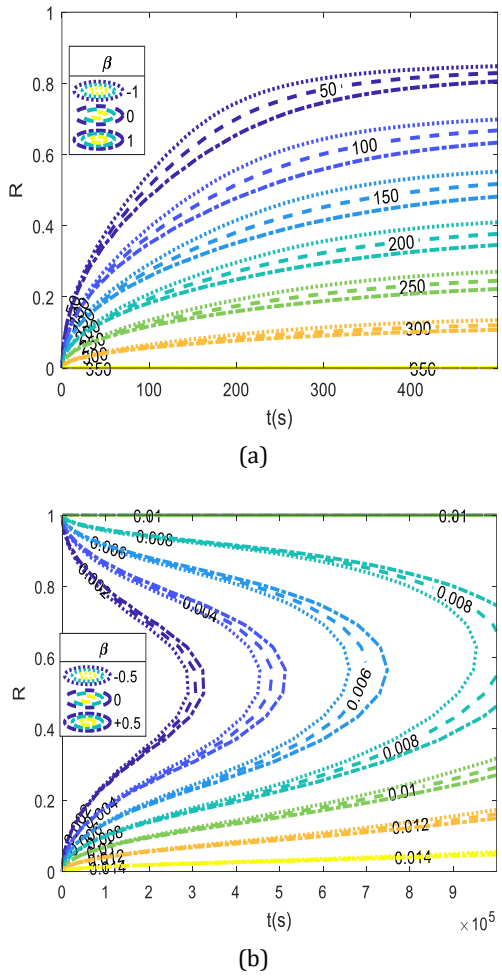

Fig. 6. Effect of inhomogeneity index on the distribution of (a) Temperature (b) Moisture, based on coupled model

4. Conclusions

The transient coupled heat transfer and moisture diffusion were considered for a short length FGM cylinder. The material constant of the cylinder was considered to vary according to a power-law function. The coupled equations of heat conduction and moisture diffusion were solved employing Fourier series expansion in the longitudinal direction, DQM in the radial direction, and the Newmark method in the time domain. According to the results, the FGM cylinder reaches the heat transfer balance earlier under the uncoupled model rather than the coupled model. Before reaching the balance, the temperature under the uncoupled model is lower than that by the coupled model. The difference between the coupled model with the uncoupled model is more obvious in moisture rather than temperature. Also, the negative grading index increases the temperature and moisture. While the effect of the positive grading index is vice versa. Moreover, for analyzing the transient hygrothermal process it is important to employ the coupled model.

Nomenclature

β	Functionally graded index
T	Temperature change [K]
M	Moisture potential change [◦M]
c_p	Heat capacity [J/kg K]
ρ	Mass density [kg/m3]
ζ	Conduction coefficient of moisture [kg/ms◦M]
ξ_d	Ratio of vapor diffusion coefficient to coefficient of total moisture diffusion
h_{LV}	Heat of phase change [kJ/kg]
L	Length of cylinder
ε	Hygrothermal index
c_m	Moisture capacity [J/kg◦M]
a, b	Inner and outer raddi [m]
k	Thermal conductivity coefficients [W/m K]
γ	Heat of absorption or desorption [kJ/kg]
$A_{ij}^{(n)}$	Weighting coefficients used for the n_{th}-order derivatives
N	Number of grid points

References

[1] Saadatfar, M. and Zarandi, M.H., 2020. Deformations and Stresses of an Exponentially Graded Magneto-Electro-Elastic Non-Uniform Thickness Annular Plate Which Rotates with Variable Angular Speed. *International Journal of Applied Mechanics, 12*(05), p. 2050050

[2] Saadatfar, M. and Zarandi, M.H., 2020. Effect of angular acceleration on the mechanical behavior of an exponentially graded piezoelectric rotating annular plate with variable thickness. *Mechanics Based Design of Structures and Machines*, pp.1-17.

[3] Saadatfar, M., Zarandi, M.H., and Babaelahi, M., 2020. Effects of porosity, profile of thickness, and angular acceleration on the magneto-electro-elastic behavior of a porous FGMEE rotating disc placed in a constant magnetic field. *Proceedings of the Institution of Mechanical Engineers, Part C: Journal of Mechanical Engineering Science, 235*(7), pp. 1241-1257.

[4] Wang, B.L. and Tian, Z.H., 2005. Application of finite element–finite difference method to the determination of transient temperature field in functionally graded materials. *Finite Elements in Analysis and Design, 41*(4), pp. 335-349.

[5] Jabbari, M., Mohazzab, A.H., Bahtui, A., Eslami, M.R., 2007. Analytical solution for

three-dimensional stresses in a short length FGM hollow cylinder. *ZAMM - Journal of Applied Mathematics and Mechanics / Zeitschrift für Angewandte Mathematik und Mechanik, 87*(6), pp. 413-429.

[6] Shao, Z.S., Wang, T.J., and Ang, K.K., 2007. Transient Thermo-Mechanical Analysis of Functionally Graded Hollow Circular Cylinders. *Journal of Thermal Stresses, 30*(1), pp. 81-104.

[7] Ootao, Y. and Tanigawa, Y., 2009. Transient Thermoelastic Problem of a Functionally Graded Hollow Cylinder Due to Asymmetrical Surface Heating. *Journal of Thermal Stresses, 32*(12), pp. 1217-1234.

[8] Asgari, M. and Akhlaghi, M., 2009. Transient heat conduction in two-dimensional functionally graded hollow cylinder with finite length. *Heat and Mass Transfer, 45*(11), pp. 1383-1392.

[9] Peng, X.L. and Li, X.F., 2010. Transient Response of Temperature and Thermal Stresses in a Functionally Graded Hollow Cylinder. *Journal of Thermal Stresses, 33*(5), pp. 485-500.

[10] Rahmati Nezhad, Y., Asemi, K., and Akhlaghi, M., 2011. Transient solution of temperature field in functionally graded hollow cylinder with finite length using multi layered approach. *International Journal of Mechanics and Materials in Design, 7*(1), p. 71.

[11] Xie, H., Dai, H.L., and Rao, Y.N., 2013. Thermoelastic Dynamic Behaviors of a FGM Hollow Cylinder Under Non-Axisymmetric Thermo-Mechanical Loads. *Journal of Mechanics, 29*(1), pp. 109-120.

[12] Nejad, M.Z. and Kashkoli, M.D., 2014. Time-dependent thermo-creep analysis of rotating FGM thick-walled cylindrical pressure vessels under heat flux. *International Journal of Engineering Science, 82*, pp. 222-237.

[13] Hosseini, M. and Dini, A., 2015. Magneto-thermo-elastic response of a rotating functionally graded cylinder. *Structural Engineering and Mechanics, 56*(1), pp. 137-156.

[14] Hosseini, M., Dini, A., and Eftekhari, M., 2017. Strain gradient effects on the thermoelastic analysis of a functionally graded micro-rotating cylinder using generalized differential quadrature method. *Acta Mechanica, 228*(5), pp. 1563-1580.

[15] Najibi, A. and Talebitooti, R., 2017. Nonlinear transient thermo-elastic analysis of a 2D-FGM thick hollow finite length cylinder. *Composites Part B: Engineering, 111*, pp. 211-227.

[16] Manthena, V.R. and Kedar, G.D., 2018. Transient thermal stress analysis of a functionally graded thick hollow cylinder with temperature-dependent material properties. *Journal of Thermal Stresses, 41*(5), pp. 568-582.

[17] Saadatfar, M., 2019. Analytical Solution for the Creep Problem of a Rotating Functionally Graded Magneto–Electro–Elastic Hollow Cylinder in Thermal Environment. *International Journal of Applied Mechanics, 11*(06), p. 1950053.

[18] Yarımpabuç, D., 2021. Transient-thermoelastic analysis of periodically rotated functionally graded hollow cylinder. *Journal of Engineering Mathematics, 128*(1), p. 18.

[19] Jabbari, M. and Nejad, M.Z., 2020. Mechanical and thermal stresses in radially functionally graded hollow cylinders with variable thickness due to symmetric loads. *Australian Journal of Mechanical Engineering, 18*(1), pp. 108-121.

[20] Dini, A., Shariati, M., Zarghami, F., Nematollahi, M.A., 2020. Size-dependent analysis of a functionally graded piezoelectric micro-cylinder based on the strain gradient theory with the consideration of flexoelectric effect: plane strain problem. *Journal of the Brazilian Society of Mechanical Sciences and Engineering, 42*(8), p. 410.

[21] Benslimane, A., Medjdoub, C., Methia, M., Khadimallah, M.A., Hammiche, D., 2021. Investigation of displacement and stress fields in pressurized thick-walled FGM cylinder under uniform magnetic field. *Materials Today: Proceedings, 36*, pp. 101-106.

[22] Saadatfar, M. and Aghaie-Khafri, M., 2014. Hygro-thermo-magneto-electro-elastic analysis of a functionally graded magnetoelectroelastic hollow sphere resting on an elastic foundation. *Smart Materials and Structures, 23*(3), p. 035004.

[23] Saadatfar, M. and Aghaie-Khafri, M., 2015. Hygrothermal analysis of a rotating smart exponentially graded cylindrical shell with imperfect bonding supported by an elastic foundation. *Aerospace Science and Technology, 43*, pp. 37-50.

[24] Saadatfar, M. and Aghaie-Khafri, M., 2015. On the Behavior of a Rotating Functionally Graded Hybrid Cylindrical Shell with Imperfect Bonding Subjected to Hygrothermal Condition. *Journal of Thermal Stresses, 38*(8), pp. 854-881.

[25] Saadatfar, M., 2015. Effect of multiphysics conditions on the behavior of an exponentially graded smart cylindrical shell with imperfect bonding. *Meccanica, 50*(8), pp. 2135-2152.

[26] Saadatfar, M., 2018. Effect of Interlaminar Weak Bonding and Constant Magnetic Field on the Hygrothermal Stresses of a FG Hybrid Cylindrical Shell Using DQM. *Journal of Stress Analysis, 3*(1), pp. 93-110.

[27] Dini, A. and Abolbashari, M.H., 2016. Hygro-thermo-electro-elastic response of a functionally graded piezoelectric cylinder resting on an elastic foundation subjected to non-axisymmetric loads. *International Journal of Pressure Vessels and Piping, 147*, pp. 21-40.

[28] Saadatfar, M., 2019. Multiphysical time-dependent creep response of FGMEE hollow cylinder in thermal and humid environment. *Mechanics of Time-Dependent Materials, 25*(2), pp. 151-173.

[29] Saadatfar, M., 2020. Stress redistribution analysis of piezomagnetic rotating thick-walled cylinder with temperature-and moisture-dependent material properties. *Journal of Applied and Computational Mechanics, 6*(1), pp. 90-104.

[30] Yang, Y.C., Chu, S.S., Lee, H.L., Lin, S.L., 2006. Hybrid numerical method applied to transient hygrothermal analysis in an annular cylinder. *International Communications in Heat and Mass Transfer, 33*(1), pp. 102-111.

[31] Dai, H.L., Zheng, Z.Q., and Dai, T., 2017. Investigation on a rotating FGPM circular disk under a coupled hygrothermal field. *Applied Mathematical Modelling, 46*, pp. 28-47.

[32] Dai, T., Ynag, Y., Dai, H.L., Tang, H., and Lin, Z.Y., 2019. Hygrothermal mechanical behaviors of a porous FG-CRC annular plate with variable thickness considering aggregation of CNTs. *Composite Structures, 215*, pp. 198-213.

[33] Peng, Y., Cheng, C.M., Chen, X.T., Zhang, X.Y., and Li, X.F., 2018. Transient hygro-thermo-elastic response in a cylinder considering non-Fourier hyperbolic heat-moisture coupling. *International Journal of Heat and Mass Transfer, 126*, pp. 1094-1103.

[34] Peng, Y., Zhang, X.Y., and Li, X.F., 2019. Transient hygrothermoelastic response in a porous cylinder subjected to ramp-type heat-moisture loading. *Journal of Thermal Stresses, 42*(12), pp. 1499-1514.

[35] Qin, M., Aït-Mokhtar, A., and Belarbi, R., 2010. Two-dimensional hygrothermal transfer in porous building materials. *Applied Thermal Engineering, 30*(16), pp. 2555-2562.

[36] Jabbari, M., Sohrabpour, S., and Eslami, M.R., 2003. General Solution for Mechanical and Thermal Stresses in a Functionally Graded Hollow Cylinder due to Nonaxisymmetric Steady-State Loads. *Journal of Applied Mechanics, 70*(1), pp. 111-118.